NANO LETTERS

Letter

Cite This: Nano Lett. 2018, 18, 5867−5874

pubs.acs.org/NanoLett

Reversible Charge-Carrier Trapping Slows Förster Energy Transfer in CdSe/CdS Quantum-Dot Solids

Federico Montanarella, Margherita Biondi, Stijn O. M. Hinterding, Daniel Vanmaekelbergh, and Freddy T. Rabouw*

Debye Institute for Nanomaterials Science, Utrecht University, P.O. Box 80000, 3508 TA Utrecht, The Netherlands

Supporting Information

ABSTRACT: The dynamics of photoluminescence (PL) from nanocrystal quantum dots (QDs) is significantly affected by the reversible trapping of photoexcited charge carriers. This process occurs after up to 50% of the absorption events, depending on the type of QD considered, and can extend the time between the photoexcitation and relaxation of the QD by orders of magnitude. Although many optoelectronic applications require QDs assembled into a QD solid, until now, reversible trapping has been studied only in (ensembles of) spatially separated QDs. Here, we study the influence of reversible trapping on the excited-state dynamics of CdSe/CdS core/shell QDs when they are assembled into close-packed "supraparticles". Time- and spectrally resolved photoluminescence (PL) measurements reveal competition among spontaneous emission, reversible charge-carrier trapping, and Förster resonance energy transfer between the QDs. While Förster transfer causes the PL to red-shift over the first 20−50 ns after excitation, reversible trapping stops and even reverses this trend at later times. We can model this behavior with a simple kinetic Monte Carlo simulation by considering that charge-carrier trapping leaves the QDs in a state with zero oscillator strength in which no energy transfer can occur. Our results highlight that reversible trapping significantly affects the energy and charge-carrier dynamics for applications in which QDs are assembled into a QD solid.

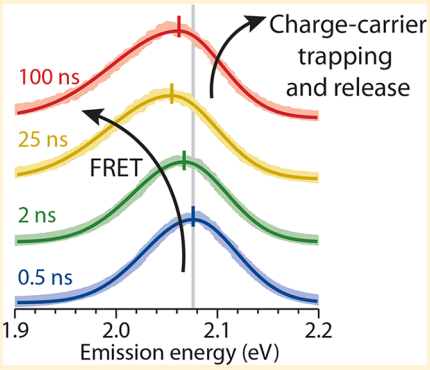

KEYWORDS: *Nanocrystal, colloidal quantum dot, charge-carrier trapping, Förster energy transfer, delayed emission*

The most-ancient application of quantum dots (QDs) reported in human history is their use for hair dyeing in ancient Greco-Roman times.[1] Since that time, significant progress has been made on the synthesis of bright and monodispersed QDs[2] as well as on the fundamental understanding of their remarkable size-dependent optoelectronic properties.[3] Nowadays QDs are used in various optoelectronic applications,[4−9] while more are still under development.[10−13] For commercial applications, QDs are usually assembled into QD solids, i.e., close-packed structures. In contrast, fundamental studies on the photophysical properties of QDs are usually performed on spatially separated QDs (for example, dispersed in solution). More in-depth studies are necessary on QDs in close-packed conditions[14−17] and on the differences in properties between spatially separated and close-packed configuration to fully understand their behavior.

It was recently shown that, upon pulsed excitation of an ensemble of separated QDs, spontaneous emission on nanosecond time scales is followed by strongly delayed emission at the same photon energies up to milliseconds after photoexcitation.[18−24] The amplitude of delayed emission in a photoluminescence (PL) decay experiment is often low, and its existence has been overlooked. However, the time-integrated delayed emission accounts for more than 10% of the overall emission for many types of QDs.[18−24] The current understanding is that the recombination of an electron−hole pair is delayed because one (or both) charge carrier is temporarily stored in a trap state. The original exciton state is restored after some time by release of the trapped charge carrier. The implications of temporary charge carrier storage on optoelectronic applications of QDs have not been addressed until now. In particular, QDs interact through charge and Förster resonance energy transfer (FRET) when assembled into a QD solid.[14−17,25] Because reversible charge-carrier trapping has such a pronounced effect on the dynamics of spontaneous emission from spatially separated QDs, a significant influence on FRET and charge transfer in QD solids can be anticipated as well.

Here, we study the effect of reversible charge-carrier trapping on the excited-state dynamics in assemblies of interacting CdSe/CdS core/shell QDs. The dynamics, and thereby the PL properties, are determined by the interplay between three processes: spontaneous emission, FRET, and temporary storage of the exciton. We use QDs with a constant CdSe core size while varying the shell thickness from 1 to 4 CdS monolayers. The QDs are assembled into supraparticles (SPs) presenting a model system of a QD solid.[26−29] The shell thickness allows us to control the FRET rate between QDs.

Received: June 22, 2018
Revised: July 27, 2018
Published: August 10, 2018

DOI: 10.1021/acs.nanolett.8b02538
Nano Lett. 2018, 18, 5867−5874

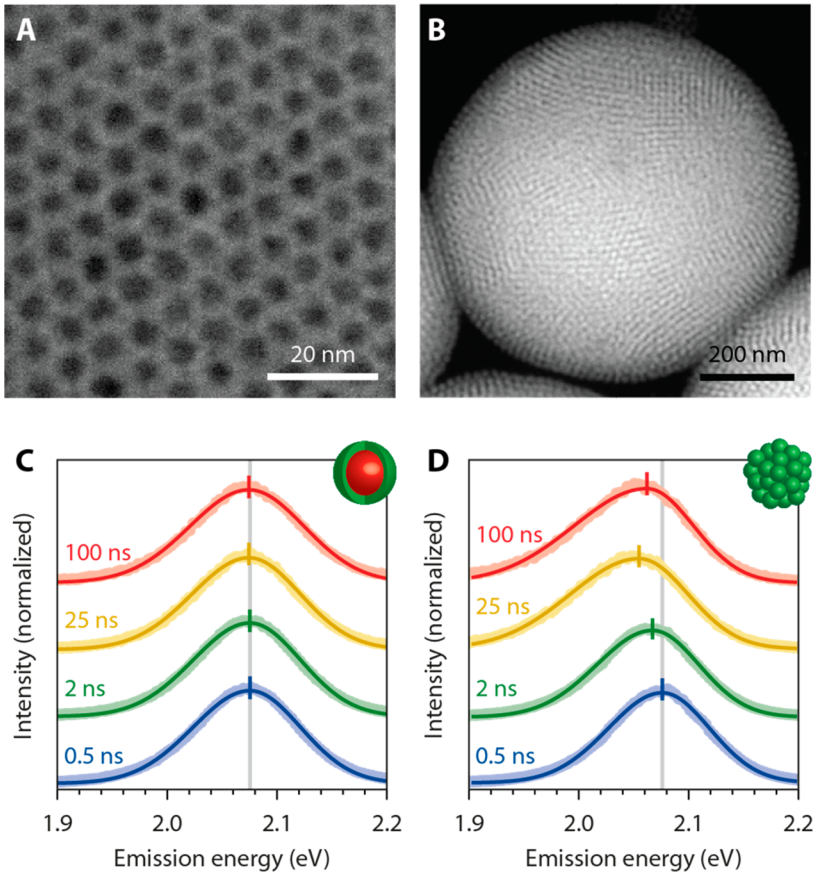

Figure 1. Energy transfer in supraparticles of quantum dots. (a) Representative transmission electron microscopy (TEM) image of the CdSe/CdS QDs. (b) Representative high-angle annular dark field scanning transmission electron microscopy (HAADF-STEM) image of a SP. (c) Emission spectra of CdSe/CdS 2 ML QDs in toluene dispersion at 0.5 ns (blue), 2 ns (green), 25 ns (yellow), and 100 ns (red) delay time after an excitation pulse. The solid lines are fits to a two-sided Gaussian (see the Supporting Information for details). The short vertical bars are the peak energies obtained. The gray vertical line is the PL peak energy of the first spectrum at 0.5 ns. (d) The same for CdSe/CdS 2 ML QDs assembled in SPs.

Our key observation is the time evolution of the PL spectrum upon pulsed excitation, recorded from the nanosecond to the microsecond time scale. We observe that the spectrum red-shifts over the first 20−50 ns after excitation, as expected for exciton diffusion by FRET, but that subsequently, this evolution stops and even reverses to a blue shift. This demonstrates the effect of reversible charge carrier storage, which temporarily freezes a QD in a state from which no FRET can occur. The release of trapped charge carrier(s) restores the exciton state. We model and reproduce the emission dynamics of our QD assemblies using kinetic Monte Carlo simulations, which we then use to track each FRET event and more quantitatively illustrate the effect of temporary charge-carrier trapping on FRET.

We synthesized QDs consisting of CdSe cores with a fixed diameter of 3.4 ± 0.3 nm (mean ± standard deviation, as determined from electron microscopy) and different CdS shell thicknesses ranging from 1 to 4 monolayers (ML). The resulting core/shell QDs have overall diameters of 3.8 ± 0.6, 4.6 ± 0.5, 5.0 ± 0.6, and 5.5 ± 0.6 nm (Figures 1a and S1). The QDs were assembled in nearly spherical supraparticles (SPs) through an oil-in-water emulsion synthesis (Figures 1b, S3, and S4).[26] Basic optical characterization of the QDs in the two configurations (freely dispersed and assembled) is shown in Figure S4. The absorption and emission spectra show a clear red shift of the first ($1S_{3/2}$−$1S_e$) exciton resonance with increasing shell thickness due to reduced quantum confinement.[30] The full width at half-maximum (fwhm) of the emission peaks is approximately 110 meV. This is wider than the line widths of 50−80 meV fwhm that have been reported for similar QDs examined at the single-QD level,[31,32] indicating some spectral broadening due to size inhomogeneity.

Following pulsed excitation of CdSe/CdS QDs with 2 ML shell thickness, we measure the time evolution of the photoluminescence (PL) spectrum over a time scale of 1 μs (Figure 1c,d). The PL spectrum shows a time-independent peak energy and line width when the QDs are dispersed in toluene (Figure 1c). In contrast, the spectra obtained for QDs assembled into SPs (Figure 1d) first shift toward lower energies (red shift) over the first 25 ns after excitation, followed by a shift toward higher energies (blue shift) at later times.

To unravel the origin of the shifts in the PL spectra of assembled QDs, we analyze the time-resolved PL measurements in more detail. In Figure 2a,b the energy of the PL emission peak is plotted as a function of delay time after excitation. The results confirm what we concluded from inspecting the PL spectra in Figure 1c,d. For the QDs dispersed in toluene (Figure 2a) the emission energy is nearly constant in time. The delayed emission at times longer than 200 ns is at slightly higher energy than the prompt emission. In contrast, in our previous experiments with another batch of QDs the delayed emission was at slightly lower energy than the prompt emission.[20] This indicates slight variations in the

DOI: 10.1021/acs.nanolett.8b02538
Nano Lett. 2018, 18, 5867−5874

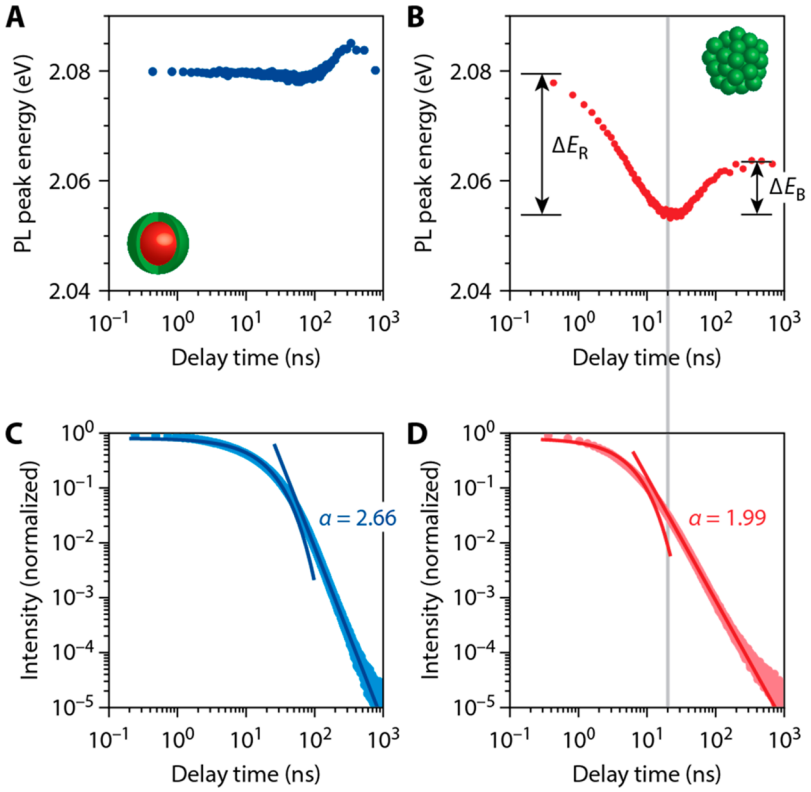

Figure 2. Time-resolved PL emission of CdSe/CdS QDs in solution and assembled in SPs. (a) PL peak energy of the CdSe/CdS 2 ML QDs dispersed in toluene as a function of delay time after the excitation pulse as obtained from two-sided Gaussian fits to the emission spectra (see the Supporting Information for details about the methods). (b) The same but for CdSe/CdS 2 ML QDs assembled in SPs. The maximum red shift, ΔE_R, and the blue shift, ΔE_B, are indicated by black arrows. (c) PL decay trace of CdSe/CdS 2 ML QDs dispersed in toluene as a function of delay time after the excitation pulse, spectrally integrated over the entire emission band, and plotted on a double-logarithmic scale. The solid lines are an exponential fit to the first part of the decay curve and the power-law fit to the later part. The delayed component has a power-law exponent of α = 2.66. (d) Same for CdSe/CdS 2 ML QDs assembled in SPs. The power-law decay has an exponent of α = 1.99. The dashed line highlights the moment when the contribution of the delayed emission becomes predominant over the prompt emission, which coincides with the reversal of the red shift in panel b.

probability of temporary carrier trapping among the QDs in ensemble. For the samples in this work, the smaller QDs may exhibit slightly more temporary trapping. The spectral dynamics are markedly different when QDs are in a close-packed configuration (Figure 2b). First, we observe a gradual redshift of the PL over the first 20 ns. This has previously been observed and studied in similar QD solids,[14−17] and can be ascribed to Förster energy transfer between adjacent QDs interacting through dipole−dipole coupling. The initial red shift is followed by a clear blue shift over 10 meV from 20 to 200 ns after excitation (Figure 2b). This blue shift has not previously been reported, although we find here that it occurs in all four QD samples under study. It reflects a likely general aspect of the excited-state dynamics in QD solids that has so far been overlooked.

To understand the PL blue shift observed for QDs assembled into SPs, we consider the (spectrally integrated) PL decay traces. For both the QDs in dispersion (Figure 2c) and for those assembled in SPs (Figure 2d), the PL decay is approximately exponential over the first tens of nanoseconds, characteristic for the "normal" spontaneous emission of excitons. The decay statistics change to power-law (straight line on a double-logarithmic scale) after the intensity drops to a few percent of the initial intensity. This power-law emission has been termed "delayed emission" and attributed to emission after temporary exciton storage by reversible trapping of charge carriers.[18−20,23] The power-law statistics (intensity proportional to $t^{-\alpha}$) reflect the wide distribution of the release times of the charge carriers from the trap states. Previous studies have demonstrated that the state with a trapped charge carrier can persist for up to milliseconds before the carrier is released,[18−20,23] the exciton state is restored, and a delayed photon is emitted. The charge-separated state (with one or both of the charge carriers localized on a trap) must have an oscillator strength orders of magnitude lower than that of the exciton state. Indeed, radiative decay, which scales linearly with oscillator strength, would otherwise limit the lifetime of the charge-separated state to much shorter than a millisecond. Interestingly, the rate of exciton diffusion by FRET scales with oscillator strength as well.[33] Hence, just as temporary charge-carrier trapping stores the exciton in separated QDs by preventing radiative recombination, so too does it prevent FRET in QD solids.

By comparing the PL decay curve of the QDs in SPs (Figure 2d) with the evolution of the PL peak position (Figure 2b), it is evident that the onset of the spectral blue shift coincides with the moment when the power-law decay component becomes dominant over the exponential component. Clearly, the delayed photons (those emitted following charge-carrier trapping and release) are less red-shifted than "normal" photons due to prompt spontaneous emission.

DOI: 10.1021/acs.nanolett.8b02538
Nano Lett. 2018, 18, 5867−5874

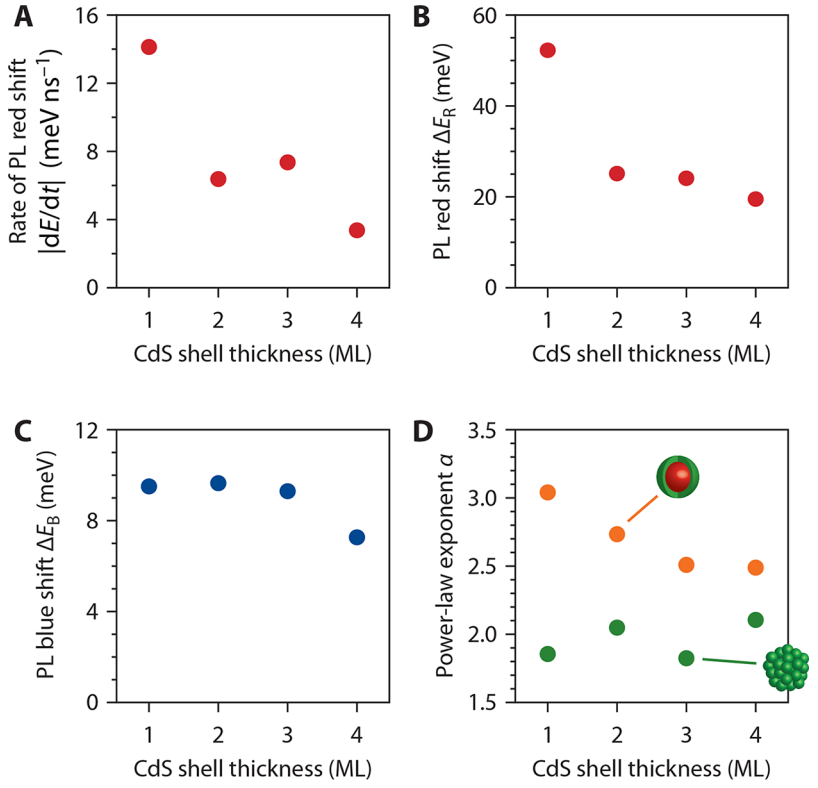

Figure 3. Analysis of the spectral dynamics as a function of shell thickness. (a) The rate of PL red shift directly after the photoexcitation of SPs as a function of the shell thickness of the constituent QDs. (b) The maximum extent of the PL red shift compared to the SP emission spectrum directly after excitation (indicated ΔE_R in Figure 2b) as a function of shell thickness. (c) The PL blue shift observed from the moment that delayed emission takes over (ΔE_B in Figure 2b) as a function of shell thickness. (d) Power-law exponent α of the delayed emission dynamics for QDs dispersed in toluene (orange) and QDs assembled in SPs (green) as a function of shell thickness.

The initial red shift and subsequent blues hift in PL energy from SPs reflects a competition between spontaneous emission, FRET, and reversible charge-carrier trapping. On the first ~20 ns after excitation, FRET gradually red shifts the PL as excitons hop from smaller QDs (with larger bandgap) to larger QDs (with smaller bandgap).[14−17] Simultaneously, charge carriers have a finite probability to be trapped in temporary traps before spontaneous emission and/or FRET can occur. Once a charge carrier is trapped, the transfer of the exciton by means of FRET is temporarily prevented. At later times, distributed from ~20 ns to at least a 1 μs after excitation (Figure 2d), the charge carrier is released, and the exciton state in the QD is restored. If temporary charge-carrier trapping had not occurred, the exciton could in the meantime have hopped to other larger QDs with red-shifted exciton energy. Reversible trapping prevents this red shift. In the experiment, this effect manifests itself in a partial reversal of the PL red shift when around ~20 ns delayed emission becomes dominant over prompt emission (Figure 2b).

The strong distance dependence of FRET (which is inversely proportional to the sixth power of the center-to-center distance) allows us to tune its interplay with spontaneous emission and reversible trapping. In Figure 3, we measure the excited-state dynamics in SPs while varying the CdS shell thickness of the constituent QDs from 1 to 4 ML. Figure 3a shows the rate of red shift of the PL, i.e., the energy red shift per unit of time ($|dE/dt|$) over the first few nanoseconds after excitation. We observe a lower rate of red shift as the shell thickness increases. Indeed, because of the strong distance dependence of FRET, we expect a lower exciton-diffusion rate[15] for increasing shell thickness. Also, the value of the red-shift ΔE_R at the moment when it reaches its maximum (around 20 ns; highlighted in Figure 2b) decreases with increasing shell thickness (Figure 3b). This is a necessary consequence of the decreasing rate of red shift with increasing shell thickness. Delayed emission becomes the dominant emission component at approximately 20 ns for all shell thicknesses (Figure S5), so the final red-shift ΔE_R at that moment scales with the rate of red-shift $|dE/dt|$. This trend still holds if we normalize the maximum red shift to the ensemble line width of the QD batch (Table S1), indicating that slight differences in the ensemble line widths of our QD batches (Table S2) do not influence the trends observed.

Interestingly, the shell thickness also affects the dynamics at times beyond 20 ns in the time regime of delayed emission due to the release of previously trapped charge carriers. The PL blue-shift ΔE_B between 20 and 200 ns shows a slight decrease with increasing shell thickness (Figure 3c). We can understand this if we realize that the blue shift reflects the energy difference between excitons that were protected from FRET by temporary storage and excitons that were free to diffuse. If diffusion is slower because of thicker shells, then the difference that temporary storage can make to the PL color is also lower.

Finally, we observe that the power-law exponent α (describing the delayed emission dynamics $I \propto t^{-\alpha}$) is affected by assembly of the QDs in SPs as well as by the shell thickness of the QDs (Figure 3d). More specifically, α is always larger for QDs freely dispersed in solution (orange) than for QDs in SPs (green). This corresponds to a wider distribution of storage times for QDs in SPs. In other words, it takes longer for the

DOI: 10.1021/acs.nanolett.8b02538
Nano Lett. 2018, 18, 5867−5874

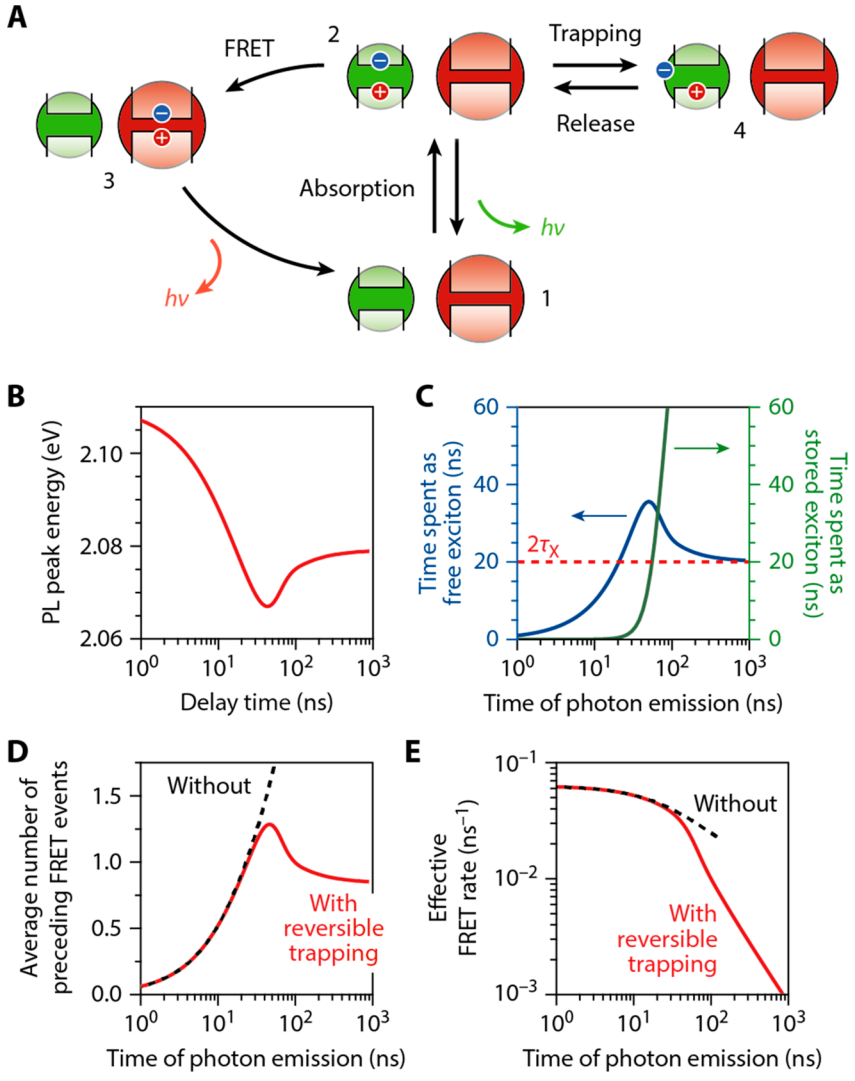

Figure 4. Kinetic Monte Carlo simulations of the excited-state dynamics in a QD solid. (a) The excited-state pathways in a QD solid considered in our model. The size inhomogeneity in a QD solid is depicted as a pair of one smaller and one bigger QD. Absorption of a photon brings the system from its ground state (state 1) into a "free-exciton" state (state 2), in which both charge carriers occupy a quantum-confined energy level. State 2 can relax back to the ground state by spontaneous emission (green arrow), the excited QD can transfer its energy to a larger neighbor by means of FRET (state 3), or one charge carrier can be trapped temporarily (state 4). State 3 may then relax by the emission of a lower-energy photon (red arrow), make a further FRET step (not depicted), or undergo temporary charge-carrier trapping (not depicted), etc. From the "stored-exciton" state (state 4), the free exciton is restored after some time by charge carrier release. More details of the model and the rates we put in are provided in the Supporting Information. (b) The simulated shifts in PL peak energy from a QD solid as a function of delay time after photoexcitation. (c) For photons emitted at time t after excitation, we track how much preceding time was spent as a free exciton (state 2 or 3 in panel a; blue) and how much time as a stored exciton (state 4; green). The dashed red line lies at twice the exciton lifetime. (d) For photons emitted at time t after excitation, we plot the number of FRET events N_{FRET} that preceded emission (red line). The black dashed line is a reference simulation without temporary trapping. (e) For photons emitted at time t after excitation, we plot the effective FRET rate $k_{FRET}^{eff} \equiv N_{FRET}/t$ during the preceding time. The black dashed line is a reference simulation without temporary trapping.

exciton state to be restored after charge-carrier trapping in SPs compared to individual QDs. Additionally, the delayed emission dynamics are more affected by QD assembly for thin-shell QDs than for those with thick shells.

We can speculate about two possible origins for the slowing of exciton restoration when QDs are assembled into SPs. First, the dielectric surrounding of QDs is different in SPs than when they are free in dispersion. In SPs, trapped charges on the surface of a QD may be stabilized by polarization of the surrounding semiconductor particles (dielectric constant of $\varepsilon \approx 10$) or water molecules ($\varepsilon = 80$) more effectively than individual QDs that are surrounded by toluene molecules ($\varepsilon = 2.4$). The improved stabilization of trapped charges will lead to a slowing of their release. This can affect the statistics of delayed emission, making late emission more likely and therefore decreasing the power-law slope α. Previous studies have indeed reported influences of the polarizability of the surrounding on the trapping dynamics of QDs.[24] Second, although exciton hopping by FRET is inhibited in the charge-separated state, charge hopping may still be possible. Exciton hopping relies on near-field electromagnetic coupling between QDs, which scales with the oscillator strength of the excited QD.[33] Charge hopping, however, is a single-carrier tunneling process, which depends, for example, on the conductivity of ligands[34] and on the Auger excitation of carriers.[35] Even if one charge carrier is (reversibly) trapped, the other carrier can still

DOI: 10.1021/acs.nanolett.8b02538
Nano Lett. 2018, 18, 5867−5874

hop from QD to QD. This could affect the dynamics of delayed emission in a QD solid. For recombination of photoexcited charges, not only must the trapped charge be released but the hopping charge must also return to the QD from which it came. This effect may contribute to a broadening of the distribution of exciton restoration times, consistent with what we observe by comparing the dynamics in SPs with those in individual QDs (Figure 3d).

Based on our experimental results, we set up a simple kinetic Monte Carlo model to understand the competition between spontaneous emission, FRET, and reversible trapping in more detail. We simulate the dynamics in a QD solid upon pulsed excitation. The processes included in the model are schematically depicted in Figure 4a for a pair of one small (green sphere) and one large QD (red sphere). The simulations are, however, done on a QD solid consisting of 864 QDs with a distribution of sizes. Following the photoexcitation of a small QD, it enters the excited state (state 2) and may directly emit (green arrow). The small QD may also transfer its energy to a larger QD by FRET (state 3), exciting the large QD and bringing the small QD back to its ground state, which eventually leads to red-shifted emission (red arrow). Alternatively, a charge carrier may be trapped, resulting in a stored-exciton state with zero oscillator strength (state 4). The trapped charge is eventually released, restoring the exciton state in the small QD, after which it can again take one of the three possible pathways (viz., spontaneous emission, energy transfer, or charge-carrier trapping). In practice, the rate of temporary charge-carrier trapping may vary among the QDs in the sample, trapping may occur not only from the emitting exciton state but also from hot-carrier states,[36,37] or some QDs in the ensemble may exhibit non-radiative recombination. We make some simplifying assumptions for our Monte Carlo model: we assign the same radiative decay rate and the same rate of temporary charge-carrier trapping to all QDs, we do not consider hot-carrier trapping,[21] and we do not include non-radiative recombination pathways. In this way, our model remains basic yet captures the relevant physics of the competition between reversible trapping, FRET, and spontaneous emission. More details of the model can be found in the caption of Figure 4a and in the Supporting Information.

The Monte Carlo model reproduces the red shift of PL on the first tens of nanoseconds followed by a blue shift at later times (compare Figure 4b to Figure 2b). As in the experiment, the transition from a red shift to a blue shift coincides with the moment that delayed emission becomes the dominant contribution to the PL. This confirms our interpretation that the spectral dynamics in SPs are a manifestation of the intricate competition between spontaneous emission, FRET, and reversible trapping.

In our Monte Carlo model, we can follow the fate of each simulated exciton in the SPs as it undergoes FRET, trapping, release, and eventually recombination by spontaneous emission. This yields insights into the competition between the different excited-state processes that are not obtainable from the experiment alone. More specifically, for the photons emitted at delay time t after photoexcitation, we can track all the steps (FRET, reversible trapping, or both) that preceded emission.

Figure 4c shows, for charge carriers recombining by photon emission at time t, how much preceding time they spent as "free exciton" (with both carriers in the quantum-confined levels of a QDs; blue) and how much was "stored exciton" (with one carrier trapped; green). The transition from prompt emission to delayed emission is clearly visible as the moment at t = 30−100 ns when the time spent as stored exciton increases from none (prompt emission) to tens of nanoseconds and further (delayed emission). Across the transition from prompt to delayed emission the time spent as free exciton first peaks at 36 ns and then levels off to 20 ns. The value of 20 ns equals twice the lifetime, τ_X, of the free-exciton state in our simulation (red dashed line). We can understand why the curve levels off to this value by considering the pathway to delayed emission, in which the system goes from the free exciton (state 2 in Figure 4a) to a stored-exciton state (state 4) back to the free-exciton state (state 2) that then decays to the ground state (state 1). The simulation also allows for the possibility of multiple reversible-trapping events, but these are relatively rare until very long delay times ($t \gg \mu$s) for the trapping probabilities relevant to our system. Each time the system is in the free-exciton state, it stays there for on average τ_X = 10 ns. Overall the system is therefore in the free-exciton state for on average twice the exciton lifetime $2\tau_X$ = 20 ns. Hence, a delayed photon emitted at time t originates from charge carriers that were free for on average a period $2\tau_X$ and stored for a period $t - 2\tau_X$.

In Figure 4d, we plot the average number of FRET events preceding emission at time t. The number of FRET events (red) peaks at 1.3 at $t \approx 40$ ns and then levels off to a value of 0.9. Clearly, the number of FRET events (Figure 4d) scales with the time that the system spends as free exciton (Figure 4c). This simply reflects that the longer the exciton is free, the more hops it makes from QD to QD. In a reference simulation without reversible trapping (black dashed line), the number of FRET events keeps increasing with time. This continuous increase is slowed and even reversed by reversible trapping (red) because this limits the time spent as free excitons.

To quantify the inhibition of FRET by reversible charge-carrier trapping, we define the "effective FRET rate" that preceded emission at time t (Figure 4e), i.e., the number of FRET events per unit of time preceding emission. The effective FRET rate slowly decreases with time t over the first 40 ns in simulations both with (red) and without (dashed line) reversible trapping. This is the result of energy disorder in a QD solid, which slows FRET as the exciton population red-shifts.[15] In addition, a pronounced effect of temporary exciton storage is observable in the delayed-emission regime (t > 40 ns): the effective FRET rate in the simulation with reversible trapping rapidly drops to a few percent of the initial rate. Hence, temporary charge-carrier trapping can slow FRET in QD solids considerably. It is this slowing of the effective FRET rate that causes the PL blue shift observed on the time scales associated with delayed emission.

In summary, we have studied the PL dynamics of QDs assembled in supraparticles on long time scales up to a microsecond. Exciton storage by reversible charge-carrier trapping is found to slow the effective rate of FRET in this system. More specifically, storage temporarily "freezes" the exciton in a state with zero oscillator strength, in which it cannot hop from QD to QD by means of FRET. For PL applications, this manifests as an effective PL blue shift at tens of nanoseconds after excitation when temporarily trapped charges are released. More generally, our work highlights that temporary charge-carrier trapping significantly affects the relaxation pathways of excited QDs. This process should be taken into account to understand the excited-state dynamics of

DOI: 10.1021/acs.nanolett.8b02538
Nano Lett. 2018, 18, 5867−5874

QDs, especially when, in QD solids, it competes with various other processes such as FRET or charge extraction.

■ ASSOCIATED CONTENT

Supporting Information

The Supporting Information is available free of charge on the ACS Publications website at DOI: 10.1021/acs.nanolett.8b02538.

Additional details in the synthesis of CdSe/CdS NCs, synthesis of the SPs, experimental setup, and analysis of the data. Images showing electron microscopy results, optical characterization, time-resolved PL emission spectra, decay traces for different shell thickness, and detailed description of the kinetic Monte Carlo simulation. Tables showing PL red shift due to FRET and contributions to the ensemble emission linewidths. (PDF)

■ AUTHOR INFORMATION

Corresponding Author

*E-mail: f.t.rabouw@uu.nl.

ORCID

Stijn O. M. Hinterding: 0000-0002-3940-1253
Daniel Vanmaekelbergh: 0000-0002-3535-8366
Freddy T. Rabouw: 0000-0002-4775-0859

Notes

The authors declare no competing financial interest.

■ ACKNOWLEDGMENTS

The authors thank A. van Blaaderen for very fruitful discussion. This work was supported by the European Commission via the Marie-Skłodowska Curie action Phonsi (H2020-MSCA-ITN-642656). D.V. acknowledges The Netherlands Organisation for Scientific Research NWO (FOM-program DDC13 and CW-Toppunt 718.015.002) and the European Research Council under HORIZON 2020 (grant no. 692691 FIRST-STEP) for financial support. F.T.R. is supported by NWO-Veni grant number 722.017.002. F.T.R. and S.O.M.H. acknowledge support from by The Netherlands Center for Multiscale Catalytic Energy Conversion (MCEC), an NWO Gravitation program funded by the Ministry of Education, Culture and Science of the government of The Netherlands.

■ REFERENCES

(1) Walter, P.; Welcomme, E.; Hallégot, P.; Zaluzec, N. J.; Deeb, C.; Castaing, J.; Veyssière, P.; Bréniaux, R.; Lévêque, J. L.; Tsoucaris, G. Early Use of PbS Nanotechnology for an Ancient Hair Dyeing Formula. *Nano Lett.* **2006**, *6*, 2215−2219.

(2) Murray, C. B.; Norris, D.; Bawendi, M. G. Synthesis and Characterization of Nearly Monodisperse CdE (E= S, Se, Te) Semiconductor Nanocrystallites. *J. Am. Chem. Soc.* **1993**, *115*, 8706−8715.

(3) Norris, D. J.; Bawendi, M. G. Measurement and Assignment of the Size-Dependent Optical Spectrum in CdSe Quantum Dots. *Phys. Rev. B: Condens. Matter Mater. Phys.* **1996**, *53*, 16338−16346.

(4) Talapin, D. V.; Lee, J. S.; Kovalenko, M. V.; Shevchenko, E. V. Prospects of Colloidal Nanocrystals for Electronic and Optoelectronic Applications. *Chem. Rev.* **2010**, *110*, 389−458.

(5) Shirasaki, Y.; Supran, G. J.; Bawendi, M. G.; Bulović, V. Emergence of Colloidal Quantum-Dot Light-Emitting Technologies. *Nat. Photonics* **2013**, *7*, 13−23.

(6) Sun, Q.; Wang, Y. A.; Li, L. S.; Wang, D.; Zhu, T.; Xu, J.; Yang, C.; Li, Y. Bright, Multicoloured Light-Emitting Diodes Based on Quantum Dots. *Nat. Photonics* **2007**, *1*, 717−722.

(7) Sukhovatkin, V.; Hinds, S.; Brzozowski, L.; Sargent, E. H. Colloidal Quantum-Dot Photodetectors Exploiting Multiexciton Generation. *Science* **2009**, *324*, 1542−1544.

(8) McDonald, S.; Konstantatos, G.; Zhang, S.; Cyr, P. W.; Klem, E. J. D.; Levina, L.; Sargent, E. H. Solution-Processed PbS Quantum Dot Infrared Photodetectors and Photovoltaics. *Nat. Mater.* **2005**, *4*, 138−142.

(9) Konstantatos, G.; Howard, I.; Fischer, A.; Hoogland, S.; Clifford, J.; Klem, E.; Levina, L.; Sargent, E. H. Ultrasensitive Solution-Cast Quantum Dot Photodetectors. *Nature* **2006**, *442*, 180−183.

(10) Grivas, C.; Li, C.; Andreakou, P.; Wang, P.; Ding, M.; Brambilla, G.; Manna, L.; Lagoudakis, P. Single-Mode Tunable Laser Emission in the Single-Exciton Regime from Colloidal Nanocrystals. *Nat. Commun.* **2013**, *4*, 1−9.

(11) Klimov, V. I.; Mikhailovsky, A. A.; Xu, S.; Malko, A.; Hollingsworth, J. A.; Leatherdale, C. A.; Eisler, H. J.; Bawendi, M. G. Optical Gain and Stimulated Emission in Nanocrystal Quantum Dots. *Science* **2000**, *290*, 314−317.

(12) Meinardi, F.; Colombo, A.; Velizhanin, K. A.; Simonutti, R.; Lorenzon, M.; Beverina, L.; Viswanatha, R.; Klimov, V.; Brovelli, S. Large-Area Luminescent Solar Concentrators Based on 'Stokes-Shift-Engineered' Nanocrystals in a Mass-Polymerized PMMA Matrix. *Nat. Photonics* **2014**, *8*, 392−399.

(13) Meinardi, F.; McDaniel, H.; Carulli, F.; Colombo, A.; Velizhanin, K. A.; Makarov, N. S.; Simonutti, R.; Klimov, V. I.; Brovelli, S. Highly Efficient Large-Area Colourless Luminescent Solar Concentrators Using Heavy-Metal-Free Colloidal Quantum Dots. *Nat. Nanotechnol.* **2015**, *10*, 878−885.

(14) Kagan, C.; Murray, C.; Nirmal, M.; Bawendi, M. G. Electronic Energy Transfer in CdSe Quantum Dot Solids. *Phys. Rev. Lett.* **1996**, *76*, 1517−1520.

(15) Akselrod, G. M.; Prins, F.; Poulikakos, L. V.; Lee, E. M. Y.; Weidman, M. C.; Mork, A. J.; Willard, A. P.; Bulovic, V.; Tisdale, W. A. Subdiffusive Exciton Transport in Quantum Dot Solids. *Nano Lett.* **2014**, *14*, 3556−3562.

(16) Crooker, S. A.; Hollingsworth, J. A.; Tretiak, S.; Klimov, V. Spectrally Resolved Dynamics of Energy Transfer in Quantum-Dot Assemblies: Towards Engineered Energy Flows in Artificial Materials. *Phys. Rev. Lett.* **2002**, *89*, 186802.

(17) Azzaro, M. S.; Dodin, A.; Zhang, D. Y.; Willard, A. P.; Roberts, S. T. Exciton-Delocalizing Ligands Can Speed Energy Migration in Nanocrystal Solids. *Nano Lett.* **2018**, *18*, 3259−3270.

(18) Whitham, P. J.; Marchioro, A.; Knowles, K. E.; Kilburn, T. B.; Reid, P. J.; Gamelin, D. R. Single-Particle Photoluminescence Spectra, Blinking, and Delayed Luminescence of Colloidal CuInS2 Nanocrystals. *J. Phys. Chem. C* **2016**, *120*, 17136−17142.

(19) Marchioro, A.; Whitham, P. J.; Knowles, K. E.; Kilburn, T. B.; Reid, P. J.; Gamelin, D. R. Tunneling in the Delayed Luminescence of Colloidal CdSe, Cu^{+}-Doped CdSe, and CuInS2 Semiconductor Nanocrystals and Relationship to Blinking. *J. Phys. Chem. C* **2016**, *120*, 27040−27049.

(20) Rabouw, F.; Kamp, M.; van Dijk-Moes, R.; Gamelin, D. R.; Koenderink, A. F.; Meijerink, A.; Vanmaekelbergh, D. Delayed Exciton Emission and Its Relation to Blinking in CdSe Quantum Dots. *Nano Lett.* **2015**, *15*, 7718−7725.

(21) Rabouw, F. T.; van der Bok, J. C.; Spinicelli, P.; Mahler, B.; Nasilowski, M.; Pedetti, S.; Dubertret, B.; Vanmaekelbergh, D. Temporary Charge Carrier Separation Dominates the Photoluminescence Decay Dynamics of Colloidal CdSe Nanoplatelets. *Nano Lett.* **2016**, *16*, 2047−2053.

(22) Sher, P. H.; Smith, J. M.; Dalgarno, P. A.; Warburton, R. J.; Chen, X.; Dobson, P. J.; Daniels, S. M.; Pickett, N. L.; O'Brien, P. Power Law Carrier Dynamics in Semiconductor Nanocrystals at Nanosecond Timescales. *Appl. Phys. Lett.* **2008**, *92*, 101111.

(23) Marchioro, A.; Whitham, P. J.; Nelson, H. D.; De Siena, M. C.; Knowles, K. E.; Polinger, V. Z.; Reid, P. J.; Gamelin, D. R. Strong

DOI: 10.1021/acs.nanolett.8b02538
Nano Lett. 2018, 18, 5867−5874

Dependence of Quantum-Dot Delayed Luminescence on Excitation Pulse Width. *J. Phys. Chem. Lett.* **2017**, *8*, 3997−4003.
(24) Jones, M.; Lo, S. S.; Scholes, G. D. Quantitative Modeling of the Role of Surface Traps in CdSe/CdS/ZnS Nanocrystal Photoluminescence Decay Dynamics. *Proc. Natl. Acad. Sci. U. S. A.* **2009**, *106*, 3011−3016.
(25) Forster, T. Energiewanderung Und Fluoreszenz. *Naturwissenschaften* **1946**, *33*, 166−175.
(26) de Nijs, B.; Dussi, S.; Smallenburg, F.; Meeldijk, J. D.; Groenendijk, D. J.; Filion, L.; Imhof, A.; Dijkstra, M.; van Blaaderen, A. Entropy-Driven Formation of Large Icosahedral Colloidal Clusters by Spherical Confinement. *Nat. Mater.* **2015**, *14*, 56−60.
(27) Vanmaekelbergh, D.; van Vugt, L. K.; Bakker, H.; Rabouw, F. T.; de Nijs, B.; van Dijk-Moes, R.; Baesjou, P.; van Blaaderen, A.; van Huis, M. A. Shape-Dependent Multiexciton Emission and Whispering Gallery Modes in Supraparticles of CdSe/Multishell Quantum Dots. *ACS Nano* **2015**, *9*, 3942−3950.
(28) Montanarella, F.; Altantzis, T.; Zanaga, D.; Rabouw, F. T.; Bals, S.; Baesjou, P.; Vanmaekelbergh, D.; van Blaaderen, A. Composite Supraparticles with Tunable Light Emission. *ACS Nano* **2017**, *11*, 9136−9142.
(29) Montanarella, F.; Geuchies, J. J.; Dasgupta, T.; Prins, P. T.; van Overbeek, C.; Dattani, R.; Baesjou, P.; Dijkstra, M.; Petukhov, A. V.; van Blaaderen, A.; et al. Crystallization of Nanocrystals in Spherical Confinement Probed by In-Situ X-Ray Scattering. *Nano Lett.* **2018**, *18*, 3675−3681.
(30) de Mello Donegá, C. Synthesis and Properties of Colloidal Heteronanocrystals. *Chem. Soc. Rev.* **2011**, *40*, 1512−1546.
(31) Cui, J.; Beyler, A. P.; Marshall, L. F.; Chen, O.; Harris, D. K.; Wanger, D. D.; Brokmann, X.; Bawendi, M. G. Direct Probe of Spectral Inhomogeneity Reveals Synthetic Tunability of Single-Nanocrystal Spectral Linewidths. *Nat. Chem.* **2013**, *5*, 602−606.
(32) Cui, J.; Beyler, A. P.; Coropceanu, I.; Cleary, L.; Avila, T. R.; Chen, Y.; Cordero, J. M.; Heathcote, S. L.; Harris, D. K.; Chen, O.; et al. Evolution of the Single-Nanocrystal Fluorescence Linewidth with Size and Shell: Implications for Exciton-Phonon Coupling and the Optimization of Spectral Linewidths. *Nano Lett.* **2016**, *16*, 289−296.
(33) Henderson, B.; Imbusch, G. F. *Optical Spectroscopy of Inorganic Solids*; Monographs on the Physics & Chemistry of the Materials; Clarendon Press: Gloucestershire, England, 2006.
(34) Kovalenko, M. V.; Scheele, M.; Talapin, D. V. Colloidal Nanocrystals with Molecular Metal Chalcogenide Surface Ligands. *Science* **2009**, *324*, 1417−1421.
(35) Shabaev, A.; Efros, A. L.; Efros, A. L. Dark and Photo-Conductivity in Ordered Array of Nanocrystals. *Nano Lett.* **2013**, *13*, 5454−5461.
(36) McGuire, J. A.; Sykora, M.; Robel, I.; Padilha, L. A.; Joo, J.; Pietryga, J. M.; Klimov, V. I. Spectroscopic Signatures of Photocharging Due to Hot-Carrier Transfer in Solutions of Semiconductor Nanocrystals under Low-Intensity Ultraviolet Excitation. *ACS Nano* **2010**, *4*, 6087−6097.
(37) Galland, C.; Ghosh, Y.; Steinbrück, A.; Sykora, M.; Hollingsworth, J. a.; Klimov, V. I.; Htoon, H. Two Types of Luminescence Blinking Revealed by Spectroelectrochemistry of Single Quantum Dots. *Nature* **2011**, *479*, 203−207.

DOI: 10.1021/acs.nanolett.8b02538
Nano Lett. 2018, 18, 5867−5874